*American Mineralogist, Volume 68, pages 426–443, 1983*

# The high-frequency vibrational spectra of vitreous and crystalline orthosilicates

BERNARD PIRIOU

*ER 60210 Elements de transition dans les solides*
*C.N.R.S. Bellevue, 1 Place Aristide Briand,*
*92190 Meudon, France*

AND PAUL MCMILLAN

*Department of Chemistry*
*Arizona State University*
*Tempe, Arizona 85287*

## Abstract

The Raman spectrum of vitreous $CaMgSiO_4$ is described in detail, and compared with that of polycrystalline monticellite, and the Raman spectra of polycrystalline forsterite, merwinite and $\beta$- and $\gamma$-$Ca_2SiO_4$ are presented. The relevant literature is reviewed to identify a consistent set of high-frequency vibrational modes for the olivines, and the assignment of these modes to $\nu_1$- and $\nu_3$-derived vibrations of the orthosilicate units is discussed. The role of vibrational mode coupling within the high-frequency band set is considered, and a simple coupling model is proposed which shows reasonable agreement with the observed spectra. Finally, tetrahedral bond lengths and angles from a number of structural refinements are examined, and some systematics are discussed in relation to the observed high-frequency spectra.

## Introduction

The olivines and related crystalline orthosilicates are of considerable importance to igneous and metamorphic petrology, and have been the subject of extensive structural studies. We have prepared polycrystalline samples of calcium magnesium orthosilicates in a solar furnace, and report their Raman spectra. We previously reported the preparation of $CaMgSiO_4$ glass (McMillan *et al.*, 1981), whose Raman spectra showed an intense polarized band at 854 $cm^{-1}$, assigned to the symmetric stretching vibration ($\nu_1$) of tetrahedral orthosilicate units.

The glass spectrum was compared with that of polycrystalline monticellite ($CaMgSiO_4$ olivine), which showed two intense bands at 852 and 817 $cm^{-1}$. These two crystal modes are derived from symmetric $\nu_1$ and asymmetric $\nu_3$ stretching vibrations of the $SiO_4$ tetrahedra (see *e.g.*, Herzberg, 1945; Servoin and Piriou, 1973). From the comparison of $CaMgSiO_4$ crystal and glass spectra, it appears that the 852 $cm^{-1}$ crystal mode should be assigned to the $\nu_1$-derived vibration. The olivines forsterite ($Mg_2SiO_4$), tephroite ($Mn_2SiO_4$) and $\gamma$-$Ca_2SiO_4$, and the orthosilicate larnite ($\beta$-$Ca_2SiO_4$), also have two intense Raman modes in the 800–850 $cm^{-1}$ region. Most previous studies have assigned the lower-frequency band to the $\nu_1$-derived vibration, in contrast to the present assignment from the $CaMgSiO_4$ glass and crystal comparison. This apparent conflict led to an examination of the vibrational spectroscopic literature on olivines, where we found a number of inconsistencies, both in observed Raman and infrared spectra and in band assignments. In the section on assignment of high-frequency modes we consider the results of the present study along with the relevant literature to identify a consistent set of high-frequency infrared and Raman bands for silicate olivines, and discuss their assignment to vibrational modes.

The isotopic exchange experiments of Pâques-Ledent and Tarte (1973) and the results of vibrational calculations suggested that $\nu_1$- and $\nu_3$-derived vibrations in the olivines might be strongly coupled. This is discussed in the section on vibrational mode coupling, where a simple coupling model is presented for Raman-active high-frequency modes, in reasonable agreement with the observed frequency shifts and relative intensity changes.

Finally, a number of studies have attempted to relate systematic changes in olivine high-frequency vibrations to compositional parameters. We have examined a number of olivine structure refinements in a search for systematics which may be correlated with the vibrational spectra. Variations in tetrahedral bond lengths and angles for olivines and related orthosilicate are considered in the section on orthosilicate crystal structures, while the relationship of these variations to the high-frequency vibrational spectra is discussed in the final section.

0003–004X/83/0304–0426$02.00

## Experimental

### *Sample preparation*

The $CaMgSiO_4$ sample was prepared from a gel, while all others were prepared from reagent-grade oxide mixes. Details of pre-fusion heating may be found in Table 1, along with analyses after melting. The samples were melted in a 2.5 kW vertical axis solar furnace at C.N.R.S. Odeillo, France. Crystalline samples were prepared by removal of the sample from the beam and allowing to cool in air. Samples for "super quench" were subjected to an initial fusion to compact the sample, then fusion followed by splat quenching onto a cooled metal surface. The quench rate by this method is estimated at $10^5$–$10^6$°C $s^{-1}$. Further details of the method are given by Coutures *et al.* (1978). Temperature at the sample could not be controlled or measured, and substantial temperature gradients must have existed. All samples were observed to melt, giving liquid globules, and glass was found in fast-quench experiments, hence it was assumed that temperatures attained were in excess of the sample melting points. Glass formation was verified by X-ray and optical examination, using a polarizing microscope.

Crystalline samples of $\beta$- and $\gamma$-$Ca_2SiO_4$, merwinite and forsterite were analyzed by electron microprobe; $CaMgSiO_4$ crystal and glass by X-ray fluorescence, and a sample of vitreous $CaMgSiO_4$ by energy-dispersive scanning electron microscopy. The results of these analyses are given in Table 1, along with experimental details of each analytical technique. Evaporation of component oxides is known to occur in solar furnace experiments, and previous work in the system CaO–MgO–$SiO_2$ (McMillan, 1981, and ms. submitted) has shown that the rate of component loss increases in the order CaO < $SiO_2$ < MgO. This is consistent with the observed sample compositions in Table 1. The $Ca_2SiO_4$ samples completely crystallized to

Table 1. Sample preparation and analysis details

| | $\beta$-$Ca_2SiO_4$ | $\gamma$-$Ca_2SiO_4$ | $Ca_3Mg(SiO_4)_2$ |
|---|---|---|---|
| | (b) | (b) | (b) |
| CaO (a) | 67.5 ± 0.7 | 67.2 ± 0.6 | 51.5 ± 2.4 |
| MgO | -- | -- | 14.8 ± 3.2 |
| $SiO_2$ | 32.5 ± 0.7 | 32.8 ± 0.6 | 33.7 ± 3.6 |

| | $CaMgSiO_4$ (crystal) | $CaMgSiO_4$ (glass) | | $Mg_2SiO_4$ | |
|---|---|---|---|---|---|
| | (c) | (c) | (d) | (b)(e) | (b)(f) |
| CaO | 33.4 ± 0.5 | 33.2 ± 0.5 | 33.7 | -- | -- |
| MgO | 32.9 ± 0.5 | 32.4 ± 0.5 | 31.8 | 67.0 ± 1.4 | 48.1 ± 8.3 |
| $SiO_2$ | 33.8 ± 0.5 | 34.3 ± 0.5 | 34.5 | 33.0 ± 1.5 | 51.9 ± 8.3 |

Oxide mixes were ground 15-30 mins. under acetone, dried 4-6 hours at 200°C, heated 6-8 hours at 1000°C. Gel mix was heated 48 hours at 1300°C, then 20 hours at 1400°C. Both were solar melted and cooled normally for polycrystalline samples. The $CaMgSiO_4$ glass was fused a second time followed by "super-quench".

Notes:

(a) Mole% oxide, normalied to 100%. Only the $Mg_2SiO_4$ crystalline sample gave poor weight % oxide sums (near 95%), presumably due to poor carbon coating at glass/crystal interfaces (e.g. Coons, 1978). All other weight % oxides summed to 98 - 102%.

(b) Electron microprobe analyses using a Cameca MS46, with 15 kV voltage and 20nA beam current. Standards were natural diopside, wollastonite, enstatite and forsterite, and data reduced with Heinrich's (1972) program FRAME. Errors are two standard deviations of around twenty points for each sample.

(c) X-ray fluorescence analyses using the low-dilution disc method of Thomas and Haukka (1978) with a Philips PW 1410 vacuum spectrometer. Errors are estimated.

(d) Analysis by energy-dispersive scanning electron microscopy (Aden and Buseck, 1979).

(e) crystalline parts of sample.

(f) coexisting inhomogeneous glass.

Table 2. Observed Raman bands for Ca, Mg orthosilicates and tephroite

| Forsterite $Mg_2SiO_4$ | | | | | Monticellite $CaMgSiO_4$ | | | Tephroite $Mn_2SiO_4$ | | |
|---|---|---|---|---|---|---|---|---|---|---|
| (a) | (b) | (c) | (d) | | (d) | (c) | | (d) | (e) | |
| 825.5 | 826 | 824.3 | 822 | $A_g$ | 817 | 817.5 | $A_g$ | 804 | 808 | $A_g$ |
| 839 | 839 | 837 | 835 | $B_{1g}$ | | | | | 820 | $B_{1g}$ |
| 856 | 856 | 856.4 | 854 | $A_g$ | 849 | 851.7 | $A_g$ | 838 | 839 | $A_g$ |
| 866 | 866 | 866 | 863 | $B_{1g}$ | | | | | | |
| 881 | 884 | 881 | 880 | $B_{2g}$ | | $884^{(1)}$ | | | | |
| 920 | 922 | 919 | 917 | $B_{3g}$ | 899 | 900<br>$\sim920^{(1)}$ | $B_{3g}$ | 891 | 892 | $B_{3g}$ |
| 966 | 966 | 965 | 960 | $A_g$ | 947 | 949.5 | $A_g$ | 932 | 935 | $A_g$ |
| 975.5 | 976 | 975 | 972 | $B_{1g}$ | | | | | | |

| $\gamma$-$Ca_2SiO_4$ | | | Larnite $\beta$-$Ca_2SiO_4$ | | | | Merwinite $Ca_3Mg(SiO_4)_2$ |
|---|---|---|---|---|---|---|---|
| (h) | (c) | | (g) | (f) | (c) | | (c) |
| | | | $818^{(2)}$ | | | | |
| 818 | 813.6 | $A_g$ | 848 | 841 | 846.8 | $A_g$ | $845^{(3)}$ |
| | | | | | | | $860^{(3)}$ |
| | | | | | | | 872 |
| 840 | 839.4 | $A_g$ | 860 | 860 | 860.7 | $A_g$ | 887 |
| | 849 | $B_{1g}$? | | 882 | 876 | $B_g$? | 911 |
| | | | | | | | 921 |
| | | | 900 | 900 | 899 | $A_g$ | 939 |
| | | | | 917 | 916.5 | $B_g$? | 980 |
| 888 | 887 | $B_{3g}$ | | | | | 991 |
| | | | 979 | 979 | 978 | $A_g$? | 1011 |
| 926 | 925 | $A_g$ | | | | | |

Notes: All frequencies are in $cm^{-1}$. (1) Due to merwinite: see text. (2) Probably due to traces of $\gamma$-$Ca_2SiO_4$. (3) Perhaps due to traces of $\beta$-$Ca_2SiO_4$.

References to Table 2: (a) Servoin and Piriou (1978); (b) Iishi (1978); (c) This study; (d) Hohler and Funck (1973); (e) Stidham et al. (1976); (f) Conjeaud and Boyer (1980); (g) Hanke and Ptaak (1978); (h) Spectrum taken by Mrs. H. Boyer; appears in applications publicity, entitled "Calcium silicates" and "Application to certain cements", for MOLE microprobe, Jobin-Yvon Instruments S.A., 16 Rue du Canal, 91160 Longjumeau, France.

silica-deficient calcium orthosilicates, while the $Mg_2SiO_4$ sample gave stoichiometric forsterite in a silica-rich glass matrix. The $CaMgSiO_4$ sample showed minor composition change, perhaps due to its preparation from a gel mix. Before any analytical work, the samples were examined by optical microscopy. The $Mg_2SiO_4$ sample was observed to contain a small amount (5–10%) of glass; all others were entirely crystalline. X-ray powder patterns were run on a Philips Norelco diffractometer from 5–60° $2\theta$, using Cu$K\alpha$ radiation. All orthosilicate patterns corresponded with the latest literature values. The X-ray pattern of $Mg_2SiO_4$ showed a broad, weak hump at low $2\theta$, probably due to the amorphous phase, while the monticellite sample was found to contain some merwinite. This is in agreement with phase equilibrium studies in the system $Mg_2SiO_4$–$Ca_2SiO_4$ (Biggar and O'Hara, 1969; Warner and Luth, 1973), which showed that monticellite is never stoichiometric $CaMgSiO_4$ at 1 atm, but is Ca-

Table 3. Source references for Figure 5(a–c)

| | | | |
|---|---|---|---|
| Olivines | | | |
| (1) | Brown (1980), Table A4, p. 362-364: from Brown (1970; Ph.D. thesis). | | |
| | Ni | $Ni_2SiO_4$ | synthetic |
| | Co | $Ca_2SiO_4$ | synthetic |
| | Kn | $(Fe_{.51}Mn_{.46}Mg_{.02})_2SiO_4$ | knebellite |
| | *Gl | $(Ca_{.49}Mn_{.46}Mg_{.05}Fe_{.004})_2SiO_4$ | glaucochroite |
| | *Ki | $(Ca_{.57}Fe_{.43})_2SiO_4$ | kirschsteinite |
| | Zn-Pi | $(Mn_{.65}Mg_{.17}Zn_{.11}Fe_{.06})_2SiO_4$ | zincpicrotephroite |
| (2) | Lager and Meagher (1978) | | |
| | Ni | $Ni_2SiO_4$ | synthetic |
| | Mo | $(Ca_{.5}Mg_{.465}Fe_{.035})_2SiO_4$ | monticellite |
| | Gl | $(Ca_{.49}Mn_{.435}Mg_{.05}Zn_{.025})_2SiO_4$ | glaucochroite |
| (3) | Brown (1980): re-refined from Birle et al. (1968) | | |
| | Fo | $(Mg_{.90}Fe_{.10})_2$ | forsterite |
| | Ho | $(Mg_{.49}Fe_{.49}Mn_{.01}Ca_{.01})_2SiO_4$ | hortonolite |
| | Fa | $(Fe_{.92}Mg_{.04}Mn_{.04}Ca_{.002})_2SiO_4$ | fayalite |
| (4) | Hazen (1976) | | |
| | *Fo | $Mg_2SiO_4$ | synthetic forsterite |
| (5) | Francis and Ribbe (1980) | | |
| | Pi | $(Mi_{.514}Mn_{.482}Ca_{.003}Fe_{.001})_2SiO_4$ | picrotephroite ($Fo_{51}$) |
| | Te | $(Mn_{.890}Mg_{.091}Ca_{.0065}Fe_{.013})_2SiO_4$ | tephroite ($Te_{91}$) |
| (6) | Brown (1980): re-refined from Onken (1965) | | |
| | Mo | $(Mg_{.5}Ca_{.5})_2SiO_4$ | monticellite |
| (7) | Hazen (1977) | | |
| | *Fa | $Fe_2SiO_4$ | synthetic fayalite |
| (8) | Czaya (1971) | | |
| | Ca | $Ca_2SiO_4$ | synthetic $\gamma$-$Ca_2SiO_4$ |
| (9) | Ghose and Wan (1974) | | |
| | | $Co_{1.10}Mg_{0.90}SiO_4$ | synthetic |
| (10) | recalculated from Smyth and Hazen (1973) | | |
| | Fo | $Mg_2SiO_4$ | synthetic forsterite |
| | Mo | $Mg_{0.75}Fe_{1.10}Mn_{0.15}SiO_4$ | hortonolite |
| (11) | Brown and Prewitt (1973). (O-O distances calculated) | | |
| | Mo | $Mg_{1.64}Fe_{0.35}Ca_{0.01}(Si_{0.99}Al_{0.01})O_4$ | lunar (12052) |
| | Mo | $Mg_{1.42}Fe_{0.58}(Si_{0.99}Al_{0.01})O_4$ | lunar (12018) |
| | Mo | $Mg_{1.38}Fe_{0.60}Ca_{0.01}Cr_{0.01}(Si_{0.99}Al_{0.01})O_4$ | (OG2B) |

deficient. Our near-$CaMgSiO_4$ stoichiometry had then crystallized monticellite plus merwinite.

After "super-quenching," the major part of the $CaMgSiO_4$ sample was crystalline: only the thinnest edges and fibers were entirely vitreous. Attempts to polish samples for Raman spectroscopy were unsuccessful due to the small size (often less than 0.5 mm) and extremely delicate nature of suitable fragments. Glass samples were selected by trial and error for those giving the most intense Raman spectrum with minimum scattering of the incident laser beam, and maximum retention of its polarization.

The excitation source for Raman spectroscopy was the 5145 or 4880Å line of a Spectra-Physics 165 $Ar^+$ laser, with scattering geometry of 90° into a Coderg PHO double monochromator. The spectra of polycrystalline samples were obtained by near-90° scattering with the incident beam at a glancing angle to the excited surface. All crystal spectra were run with resolving slits of 2 $cm^{-1}$, while 6 $cm^{-1}$ slits were used for the glass spectra. Finally, the spectrum of merwinite was obtained with a Coderg triple monochromator in the Laboratoire d'Optique Appliquée, ENSTA, Palaiseau, using similar conditions to those described above.

## Experimental results

The high-frequency (>800 $cm^{-1}$) lattice modes of the olivines may be described in terms of coupled stretching vibrations of the four $SiO_4$ tetrahedra in the unit cell. The expected high-frequency Raman-active modes may be obtained by factor-group analysis (*e.g.*, Fateley *et al.*, 1972). Eight bands are expected, two derived from the symmetric $\nu_1$ vibration of the isolated tetrahedron, and six from its asymmetric stretch $\nu_3$. One $\nu_1$-derived mode

Table 3. (continued)

| | | | | | |
|---|---|---|---|---|---|
| (12) | Smyth (1975). (O-O distances calculated) | | | | |
| | *Fa | $Fe_2SiO_4$ | | | synthetic |
| (13) | Rajamani et al. (1975). (O-O; O-Si-O calculated) | | | | |
| | | $Ni_{1.03}Mg_{0.97}SiO_4$ | | | synthetic |
| (14) | Morimoto et al. (1974) | | | | |
| | * | $Co_2SiO_4$ | | | synthetic |
| (15) | Basso et al. (1975). Ten natural (Mg,Fe) olivines. | | | | |
| | | 3G9 | $Fo_{91.5}$ | 3G19 | $Fo_{91}$ |
| | | 3G12 | $Fo_{90.5}$ | 3G51 | $Fo_{91}$ |
| | | 3G15 | $Fo_{90.5}$ | 2488 | $Fo_{93.5}$ |
| | | 3G17 | $Fo_{89.5}$ | 2500 | $Fo_{91}$ |
| | | 3G18 | $Fo_{92.5}$ | 2501 | $Fo_{91}$ |
| (16) | Wenk and Raymond (1973). Four natural (Mg,Fe) olivines. | | | | |
| | | $(Mg_{0.95}Fe_{0.012}Mn_{0.003})_2SiO_4$ | | | Yosemite 103-481 |
| | | $(Mg_{0.893}Fe_{0.099}Ni_{0.008})_2SiO_6$ | | | Bergell Alps Sci 59 |
| | | $(Mg_{0.672}Fe_{0.319}Ni_{0.004}Ca_{0.005})_2SiO_4$ | | | Apollo 12 |
| | | $(Mg_{0.637}Fe_{0.358}Ca_{0.005})_2SiO_4$ | | | Apollo 11 |
| (17) | Finger (1970). Two natural (Mg,Fe) olivines. | | | | |
| | | $(Mg_{1.463}Fe_{0.529}Ca_{0.008})_2SiO_4$ | | | 10020 |
| | | $(Mg_{0.98}Fe_{1.013}Ca_{0.007})_2SiO_4$ | | | C15-16 |
| (18) | Hanke (1965) | | | | |
| | Fo | $(Mg_{0.9}Fe_{0.1})_2SiO_4$ | | | natural forsterite |
| | Fa | $Fe_2SiO_4$ | | | natural fayalite |
| Non-olivines | | | | | |
| (19) | Cruickshank (1964): re-refined from Midgley (1952) | | | | |
| | *La | $Ca_2SiO_4$ | | | synthetic $\beta$-$Ca_2SiO_4$ |
| (20) | Yamaguchi and Suzuki (1967) (distances and angles calculated) | | | | |
| | Mw | $Ca_3Mg(SiO_4)_2$ | | | synthetic merwinite |
| (21) | Moore and Araki (1972). (O-Si-O calculated) | | | | |
| | Mw | $Ca_3Mg(SiO_4)_2$ | | | synthetic merwinite |

Note: *denotes refinements not used for Figure 5, as discussed in text.

is of $A_g$ symmetry, as are two $\nu_3$-derived vibrations. Correlated with these three $A_g$ modes by the unit cell symmetry (Davydov splitting) are three $B_{1g}$ modes, one from $\nu_1$, and two from $\nu_3$. The two remaining $\nu_3$-derived modes have $B_{2g}$ and $B_{3g}$ symmetry (see Table 4, and Servoin and Piriou, 1973).

The observed crystal spectra are displayed in Figures 1 and 2; the left side of the figure showing the complete spectra to near 1000 $cm^{-1}$, while on the right appear details of the high frequency region. It may be seen that the frequency range covered by the high-frequency modes, due mainly to the site-group splitting of $\nu_3$-derived vibrations, is around 100 $cm^{-1}$, much larger than the Davydov splitting ($A_g$–$B_{1g}$) which is never more than 15 $cm^{-1}$. The site-group splitting appears generally to decrease in the order forsterite (Fo) > monticellite (Mo) > $\gamma$-dicalcium silicate ($\gamma$-$C_2S$), while the relative intensities of the two strongest modes change continuously in the same sequence. These observations form the basis for much of the discussion in the present report.

Figure 1a shows the Raman spectrum of polycrystalline forsterite, $Mg_2SiO_4$. The vibrational mode symmetries have been assigned from the single crystal studies of Servoin and Piriou (1973) and Iishi (1978). The $B_{3g}$ and $B_{2g}$ modes at 919 and 881 $cm^{-1}$ are readily attributed to $\nu_3$-derived vibrations, as may be the high-frequency $A_g$ mode at 965 and its related $B_{1g}$ at 975 $cm^{-1}$. However, the attribution of the $A_g$ modes at 824 and 856 $cm^{-1}$, and their correlated $B_{1g}$ modes at 837 and 866 $cm^{-1}$, to $\nu_1$- and $\nu_3$-derived vibrations is not evident.

The Raman spectrum of polycrystalline monticellite appears in Figure 1b. The spectrum is comparable with the single-crystal study of Hohler and Funck (1973), except for the band at 884 and the weaker feature near 920 $cm^{-1}$. These are due to bands of merwinite which was identified as an impurity from the X-ray pattern. The monticellite band symmetries have been taken from the work of Hohler and Funck. Only the three $A_g$ modes and the single $B_{3g}$ were distinguished in both their study and the present work. The $B_{3g}$ at 900 and $A_g$ at 949 $cm^{-1}$ may

Table 4. Factor group analyses for larnite ($\beta$-$Ca_2SiO_4$) and merwinite ($Ca_3MgSi_2O_8$), and summarized for olivine ($M_2TO_4$)

**Larnite** $\beta$-$Ca_2SiO_4$: Midgley (1952); Cruikshank (1964). Monoclinic space group $P2_{1/n}$ ($C^5_{2h}$); z = 4 (28 atoms). All atoms in general positions 4(e) of symmetry $C_1$. Total modes: $\Gamma^M = 21\ A_g + 21\ A_u + 21\ B_g + 21\ B_u$. Infrared active: $20\ A_u + 19\ B_u$; Raman active: $21\ A_g + 21\ B_g$.

Site analysis at $\underline{k} = \underline{0}$:

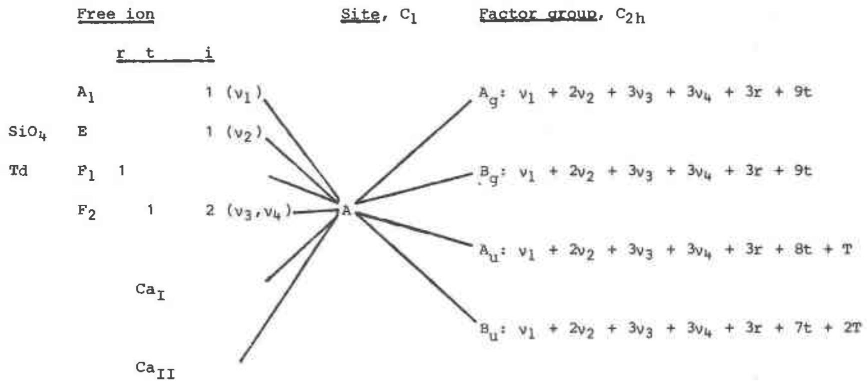

(T denotes acoustic mode)

Raman active high-frequency internal modes:

$$\nu_1 \longrightarrow A_g + B_g$$

**Merwinite** $Ca_3Mg(SiO_4)_2$: Yamaguchi and Suzuki (1967); Moore and Araki (1972): monoclinic space group $P2_{1/a} = C^5_{2h}$; z = 4 (56 atoms).

point group 2/m = $C_{2h}$

All atoms in general positions 4(e) of symmetry $C_1$.

The factor group analysis is identical to that for larnite with twice as many vibrational degrees of freedom.

Total vibrations: $\Gamma^M = 42\ A_g + 42\ A_u + 42\ B_g + 42\ B_u$

Infrared active: $41\ A_u + 40\ B_u$; Raman active: $42\ A_g + 42\ B_g$

Raman active high-frequency internal modes of $SiO_4$

$$\nu_1 \longrightarrow 2A_g + 2B_g$$
$$\nu_3 \longrightarrow 6A_g + 6B_g$$

**Olivine structure** $M_2TO_4$: see Table 3, and Servoin and Piriou (1973) for factor group analysis.

Orthorhombic space group Pbnm ($C^{16}_{2n}$), z = 4.

Total modes: $\Gamma^M = 11\ A_g + 7\ B_{1g} + 11\ B_{2g} + 7\ B_{3g} + 10\ A_u + 10\ B_{2u} + 14\ B_{3u}$

Raman active high-frequency internal modes:

$$\nu_1 \longrightarrow A_g + B_{1g} + B_{2g} + B_{3g}$$
$$\nu_3 \longrightarrow 2A_g + 2B_{1g}$$

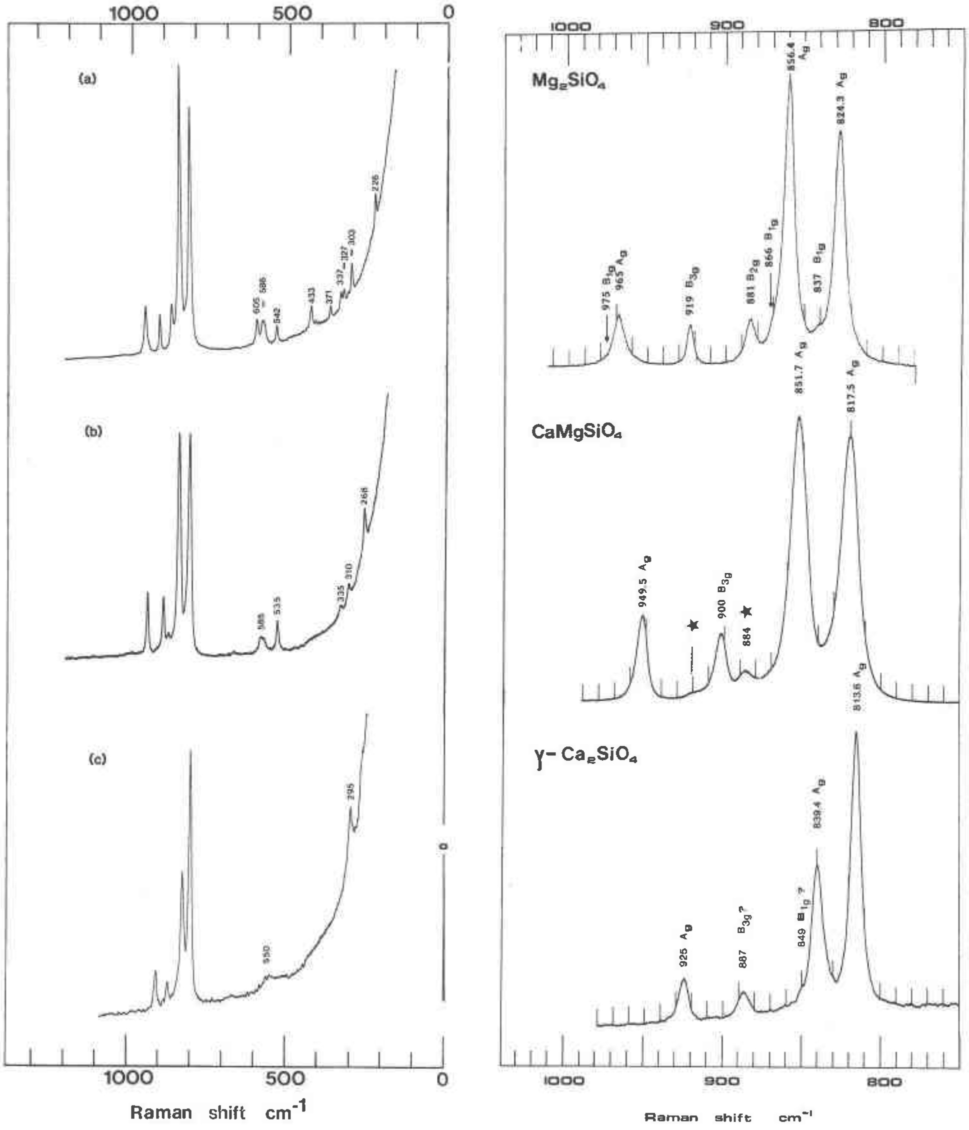

Fig. 1. Raman spectra of polycrystalline (a) forsterite, (b) monticellite and (c) $\gamma$-$Ca_2SiO_4$. Overall spectra on left, and detail of high-frequency bands on right. Bands marked (*); see Table 2 and text.

be attributed to $\nu_3$-derived vibrations. However, as for forsterite, the $A_g$ bands at 852 and 817 may not easily be assigned.

Figure 1c shows the Raman spectrum of $\gamma$-$Ca_2SiO_4$, which compares well with one obtained by H. Boyer in the Jobin-Yvon Applications Laboratory (see notes to Table 2 for full reference). Its spectrum may be partly assigned by comparison with those of forsterite and monticellite. The bands at 925 and 887 $cm^{-1}$ are probably $A_g$ and $B_{3g}$ modes derived from $\nu_3$, while the weak shoulder at 849 $cm^{-1}$ may be a $B_{1g}$ mode related to the $A_g$ band at 839 $cm^{-1}$, or could be the expected $B_{2g}$ mode. Once more, the problem arises of assigning the strong $A_g$ modes at 839 and 814 $cm^{-1}$ to $\nu_1$- and $\nu_3$-derived vibrations. Finally, we note a similar assignment problem in the spectrum of tephroite, ($Mn_2SiO_4$), which has two intense $A_g$ bands at 839 and 808 $cm^{-1}$ (Stidham *et al.*, 1976).

Figure 2 presents the Raman spectra of larnite and merwinite. That of $\beta$-$Ca_2SiO_4$ is similar to spectra obtained by Conjeaud and Boyer (1980), and by Handke and Ptaak (1978). Larnite has a monoclinic unit cell based on the $K_2SO_4$ structure (Midgley, 1952; Cruickshank, 1964; Eysel and Hahn, 1970), while merwinite is also monoclinic, and related to the larnite structure (Yamaguchi and Suzuki, 1967; Moore and Araki, 1972). A factor group analysis for $\beta$-$Ca_2SiO_4$ is shown in Table 4. Eight high-frequency, Raman-active internal modes are expected;

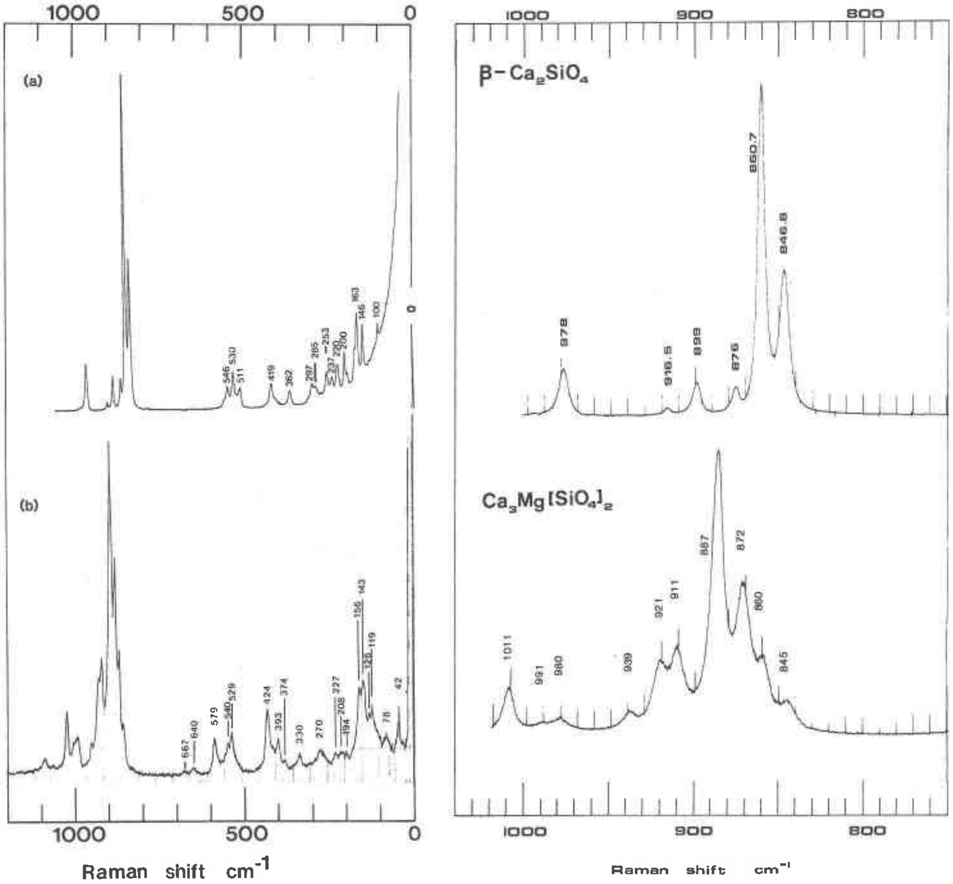

Fig. 2. Raman spectra of polycrystalline (a) larnite and (b) merwinite. Overall spectra on left, and detail of high-frequency bands on right.

four of $A_g$ symmetry and four $B_g$ modes, each correlated with an $A_g$ mode by the Davydov splitting. One $A_g$, $B_g$ pair is derived from the $\nu_1$ vibration, and the three remaining pairs from $\nu_3$. No assignment of band symmetries may be made from the single crystal study of Handke and Ptaak (1978), and their band at 818 cm$^{-1}$ does not appear in our spectrum and is probably due to some γ-$Ca_2SiO_4$ phase as impurity. On the basis of relative intensities, we have tentatively assigned the bands of β-$Ca_2SiO_4$ at 978, 899, 861 and 847 cm$^{-1}$ to $A_g$ modes. The weaker bands at 917 and 876 have then been assigned to $B_g$ modes correlated with the $A_g$ modes at 899 and 861 cm$^{-1}$ respectively. This gives a Davydov splitting of 16 cm$^{-1}$, comparable with that found for the olivines above, and supporting this assignment. The $A_g$ band at 978 and the $A_g$, $B_g$ pair at 899 and 917 may be attributed to $\nu_3$-derived vibrations. However, as in the olivines, the assignment of the $A_g$, $B_g$ pair at 861 and 876 and the $A_g$ at 847 to the remaining $\nu_3$- and $\nu_1$-derived vibrations is not evident. The factor group analysis for merwinite is also described in Table 4, and is identical to that for larnite, but with the number of vibrational modes doubled. The three bands at 860, 845 and 980 cm$^{-1}$ in the merwinite spectrum could be due to a trace of β-$Ca_2SiO_4$ impurity. No attempt has been made to assign band symmetries, although the strong bands at 887 and 872 cm$^{-1}$ are probably $A_g$ modes.

The polarized spectrum of vitreous $CaMgSiO_4$ (McMillan *et al.*, 1981) is reproduced in Figure 3, compared with the spectrum of polycrystalline monticellite. Due to the nature of the glass sample, which prevented polishing of plane faces for Raman study, the two polarizations may not be pure, and some mixing of VV and VH spectra may be present. Assignment of the observed bands is discussed in the next section.

## Discussion

### *The spectrum of $CaMgSiO_4$* glass

The spectrum consists of an intense, highly-polarized band at 854 cm$^{-1}$, with a very broad, depolarized, high-frequency shoulder of medium intensity (Figs. 3, 4). A weak, polarized band occurs at 704 cm$^{-1}$, and a weak doublet with maxima near 580 and 530 cm$^{-1}$, of which the

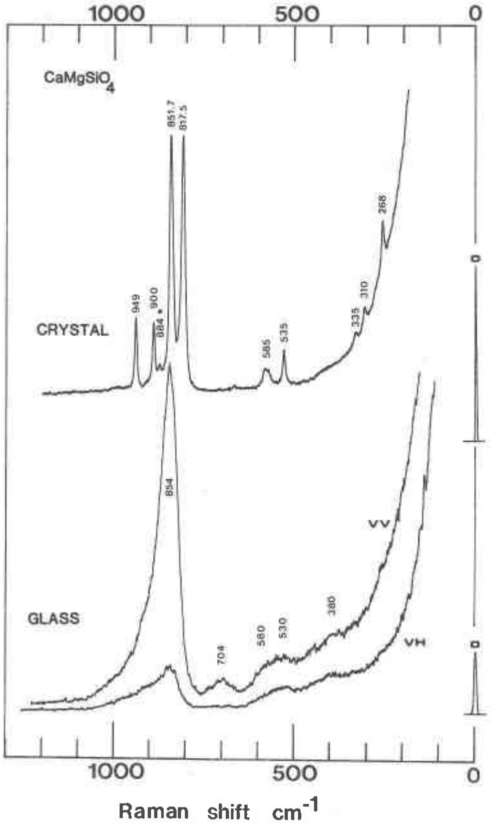

Fig. 3. Raman spectrum of polycrystalline monticellite (top) and polarized spectra of vitreous $CaMgSiO_4$ (bottom).

higher-frequency component is more polarized (Fig. 3) (McMillan *et al.*, 1981).

Infrared spectra of orthosilicate crystals (*e.g.*, Tarte, 1963); Servoin and Piriou, 1973) suggest that bands derived from the $\nu_3$ vibration occur between 850 and 1000 $cm^{-1}$, while weak sharp peaks in the 800–850 $cm^{-1}$ region have been attributed to $\nu^{-1}$. Raman spectra of aqueous silicate solutions (Fortnum and Edwards, 1956) showed a band near 777 $cm^{-1}$, which was assigned to $\nu_1$ of hydrated $SiO_4$ groups. (A band at 935 $cm^{-1}$ was observed, which was associated with the $SiO_4$ vibrations. It is tempting to assign this to the $\nu_3$ vibration, but our unpublished preliminary data on aqueous silicate solutions suggest that this region is complicated by vibrations of higher silicate polymers.) Considering all these data we expected a strong Raman band in the 800–850 $cm^{-1}$ region for the symmetric $\nu_1$ vibration of isolated $SiO_4$ tetrahedra in our $CaMgSiO_4$ glass. This band has $A_1$ symmetry, and should be completely polarized. A broadened, depolarized band was expected at higher frequency for components of the $\nu_3$ vibration, of $F_2$ symmetry. We have assigned the strong, polarized band observed at 854 $cm^{-1}$ to the $\nu_1$ vibration of the isolated $SiO_4$ unit, and its depolarized, high frequency shoulder mainly to $\nu_3$-type vibrations.

In an orthosilicate glass, the $SiO_4$ tetrahedra vibrate nearly independently in the absence of translational symmetry. The $A_1$ band at 854 $cm^{-1}$ in $CaMgSiO_4$ glass is then a $\nu_1$ vibration of an isolated $SiO_4$ tetrahedron, perturbed by interaction with $Ca^{2+}$ and $Mg^{2+}$. Crystal modes derived from coupling of $\nu_1$ vibrations within the unit cell might be expected to have a similar frequency to the free ion $\nu_1$ if the tetrahedron were not too distorted and coupling of $\nu_1$ and $\nu_3$ motions were minimal. However, phonons derived from combination of $\nu_3$ motions should have no counterpart in the glass spectrum, being a function of the crystal symmetry.

It may be seen from Figure 3 that the $\nu_1$ band of $CaMgSiO_4$ glass corresponds closely with the $A_g$ mode at 852 $cm^{-1}$ of monticellite. This suggests the assignment of this $A_g$, and its associated $B_{1g}$ mode (not observed) to $\nu_1$-derived vibrations. This is also suggested by Figure 4, which shows the behavior of the high-frequency bands as $CaMgSiO_4$ glass is crystallized by laser heating. The 854 $cm^{-1}$ band appears common to crystal and glass, while

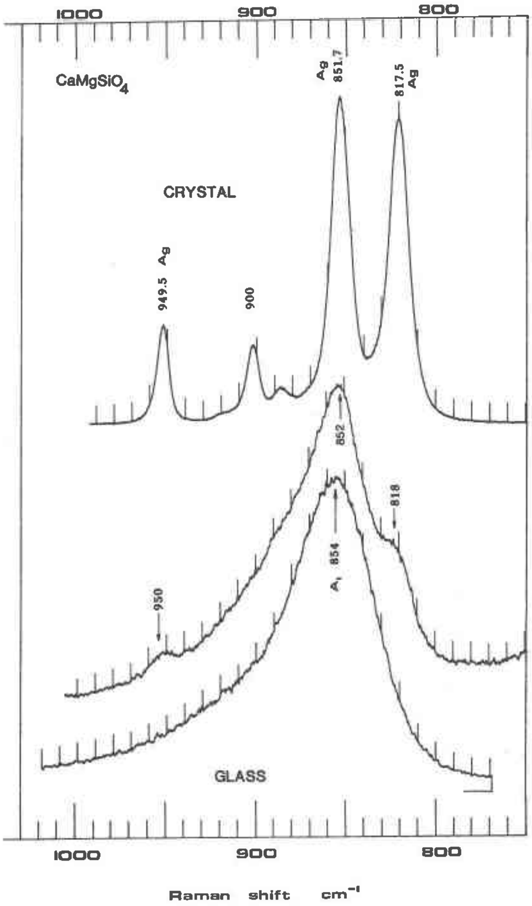

Fig. 4. High-frequency detail of Raman spectrum of polycrystalline monticellite (top) and VV spectrum of $CaMgSiO_4$ (bottom). Sequence bottom to top follows the spectral changes on crystallization of the glass sample by laser heating.

the others appear to grow as crystallization proceeds, suggesting the attribution of the 853 $cm^{-1}$ $A_g$ mode to a $\nu_1$-derived vibration. This is discussed more fully in the following sections.

The weak double band at 520–600 $cm^{-1}$ in the glass may be partly assigned to the asymmetric deformation $\nu_4$ of the $SiO_4$ tetrahedron, by comparison with the crystal spectrum. The weak, polarized band at 704 $cm^{-1}$ has no counterpart in the crystal spectrum. No bands are expected in this region for modes of $SiO_4$ units, and vibrations of Ca–O or Mg–O linkages are expected at much lower frequencies (*e.g.*, Lazarev (1972) p. 174–175; Nelson and Exarhos, 1979). The most probable attribution is to the symmetric stretch of Si–O–Si groups in higher silicate polymer species. A polarized band occurs in the region 700–600 $cm^{-1}$ in crystalline pyrosilicates; its frequency dependent on the Si–O–Si angle and the cation–oxygen bonding (*e.g.* Lazarev (1972) p. 66–69; Bretheau-Raynal *et al.*, 1979). A weak band was observed near 700 $cm^{-1}$ by Mysen *et al.* (1980) and McMillan (1981, and ms. submitted) in glasses of composition near $CaMgSiO_4$, increasing in intensity with increasing silica content. This assignment implies the presence of stretch bands due to higher silicate polymers in the region 900–1000 $cm^{-1}$. These contributions may exist, but would be masked by the $SiO_4$ vibrations. Consistent with this, the glass analysis showed the $SiO_2$ content to be slightly high, due to loss of MgO component by evaporation (Table 1). Finally, the weak depolarized band near 380 $cm^{-1}$ may be partly due to Ca–O vibrations. A similar feature has been observed in other Ca-containing oxide glass systems (*e.g.*, Mysen *et al.*, 1980; McMillan, 1981, and ms. submitted). We suggest that part of the double band at 530 and 580 $cm^{-1}$ might be due to MgO vibrations, but have no confirmation for this.

We are not aware of any other work on calcium or magnesium orthosilicate glasses, but a number of Raman studies have been carried out on basic CaO–$SiO_2$ and MgO–$SiO_2$ glasses (Mysen *et al.*, 1980; Virgo *et al.*, 1980; Kashio *et al.*, 1980; McMillan, 1981, and ms. submitted). All observed a sharp, polarized band at 850–860 $cm^{-1}$ whose intensity decreased rapidly with increasing silica content, and which may be attributed to the $\nu_1$ vibration of isolated $SiO_4$ tetrahedra in these systems. The frequency of this vibration seems to vary little on substitution of Mg for Ca, which is of interest for the later discussion of variation of band frequencies with composition in crystalline orthosilicates.

Kusabiraki and Shiraishi (1981) have reported the IR powder transmission spectrum of vitreous $Fe_2SiO_4$. They find a strong, broad band centered near 900 $cm^{-1}$ for $\nu_3$ vibrations of the isolated tetrahedra, consistent with the above discussion of $CaMgSiO_4$ glass. However, these authors assign a weak IR band at 695 $cm^{-1}$ to the $\nu_1$ vibration, which seems unjustified in view of the IR and Raman work on crystalline fayalite, where $\nu_1$ is identified at 832 $cm^{-1}$. Unlike the Raman spectrum, the non-polar $\nu_1$ mode should not appear in the IR absorption, but if present, would be expected as a weak shoulder in the 820–860 $cm^{-1}$ region. Their 695 $cm^{-1}$ band is probably related to vibrations of more polymerized silicate species. These polymers will also contribute to the high frequency part of the $Fe_2SiO_4$ glass infra-red spectrum reported by Kusabiraki and Shiraishi.

### *Orthosilicate crystal structures*

Before beginning the discussion of the vibrational spectra of the olivines and related orthosilicates, it is necessary to consider their crystal structures. The olivine structure has been described in detail by Brown (1980). The near-octahedral cation sites are distorted, and are split into two populations; the M(1) and M(2) sites. The tetrahedral sites T are also distorted. Much effort has been devoted to investigating the systematics of and reasons for these distortions. Such studies are far from being conclusive or concluded, and are reviewed by Brown (1980).

One point noted by Brown (p. 314) is that, for all silicate olivines studied, the average tetrahedral Si–O distance is remarkably constant, and that neither this nor individual Si–O distances correlated with octahedral cation size. In the present study, tetrahedral bond lengths and angles from forty olivine refinements were compared (see Table 3 for data sources). As already noted by several authors, (*e.g.*, Birle *et al.*, 1968; Louisnathan and Gibbs, 1972) the longest bond is generally Si–O(2), and the shortest Si–O(1). Some structural analyses quoted in Table 3 deviate from this; Smyth's (1975) and Hazen's (1977) refinements for fayalite, and Brown (1980) (from Brown, 1970) for kirschsteinite. The analysis for kirschsteinite has not been repeated and may be correct, but the fayalite refinements do not agree with those of Birle *et al.* (1968) or Hanke (1965), and have not been considered in this study. Hazen's (1976) analysis for forsterite, and the $Co_2SiO_4$ analysis of Morimoto *et al.* (1974), are likewise incompatible with the general trends, having a much lower Si–O(2) distance than those of other similar refinements. Finally, Brown's (1970) (see Brown, 1980) refinement for glaucochroite is not consistent with that of Lager and Meagher (1978), nor with the overall trend, and has likewise been ignored. The analysis of Czaya (1971) was used for $\gamma$-$Ca_2SiO_4$.

On examination of the 34 olivine refinements considered, it was observed that not only the average Si–O distance, but the individual tetrahedral lengths and angles were similar, apart from those for $\gamma$-$Ca_2SiO_4$. Since the only difference between $\gamma$-$Ca_2SiO_4$ and the other olivines is the presence of Ca on the M(1) site, the M(1) cation was used as a differentiating parameter. The size of the M(1) site was taken as the average value of M(1)–O distances, and Figure 5 shows plots of tetrahedral Si–O and O–O lengths and O–Si–O angles versus <M(1)–O>. All lines drawn have been fitted to the data by linear regression excluding $\gamma$-$Ca_2SiO_4$. It is emphasized that these plots are not intended to have a structural significance, but are to allow differentiation of $\gamma$-$Ca_2SiO_4$ from the other olivines by plotting of tetrahedral parameters on a common scale. No attempt was made to separate the trends of the angles and edges involving the apical oxygen O(1): these were each treated as one population with a generally decreasing trend. In $\gamma$-$Ca_2SiO_4$ unlike the other olivines, the lengths Si–O(2) and Si–O(3), the edges O(2) and O(3), and the angles O(2)–Si–O(3) and O(3)–Si–O(3), are all nearly equal. This gives the $SiO_4$ unit nearly $C_{3v}$ symmetry: much higher than the $C_s$ encountered in the other olivines. This may be partly due to the large size of $Ca^{2+}$ tending to "equalize" the two M sites, and minimizing their differences in polyhedral edge-sharing effects.

Several workers have examined the effects of polyhedral edge sharing on polyhedral distortions in the olivine structure, and on bonding in general (reviewed by Brown (1980), p. 329–334). It appears that a high degree of edge-sharing involves generally longer bonds in the component polyhedra. Merwinite is an orthosilicate with no tetrahedral–octahedral edge-sharing, as opposed to the olivines (Moore and Araki, 1972). Its tetrahedral parameters have been plotted on the right side of Figure 5, on the same scale as the olivines. It may be seen that the merwinite Si–O bond lengths are generally shorter than those of the olivines. The structure of $\beta$-$Ca_2SiO_4$ was determined by Midgley (1952), and re-refined by Cruickshank (1964), but is not good enough for direct comparison with the olivine and merwinite parameters plotted in Figure 5. (In fact, Midgley (1952, p. 312) stated that the oxygen positions were not exactly fixed from the experimental data, and that quoted bond lengths were not particularly significant.) However, from the refinements, and the drawing of Eysel and Hahn (1970), it may be seen that the $SiO_4$ units in $\beta$-$Ca_2SiO_4$ share only one edge (O(3)–O(4)) with the $CaO_6$ octahedron. This is much less edge-sharing than in the olivines, and might suggest a shorter average Si–O distance than in $\gamma$-$Ca_2SiO_4$.

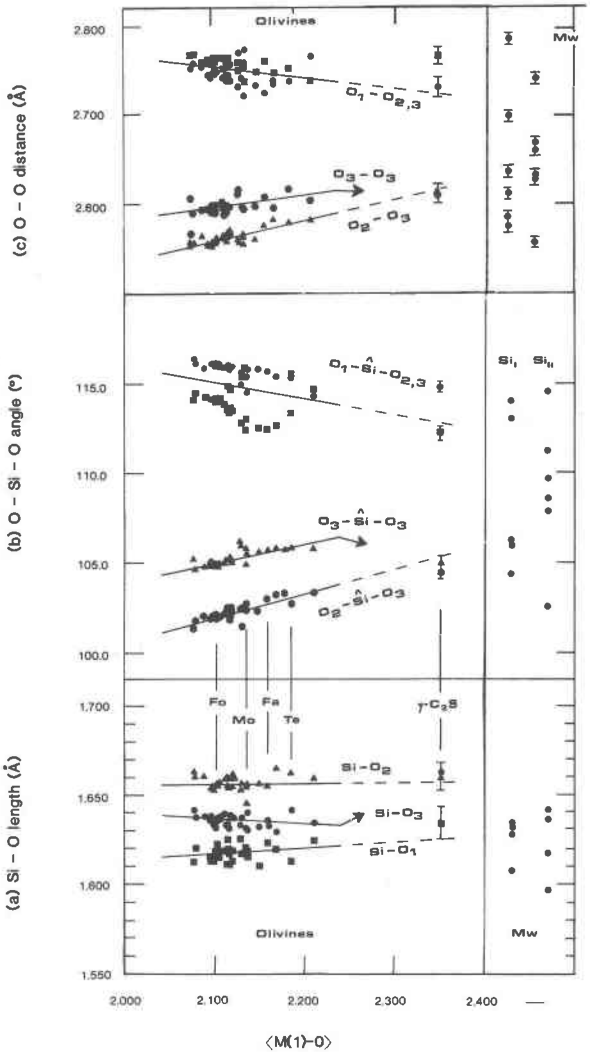

Fig. 5. Variation with ⟨M(1)–O⟩ of olivine tetrahedral distances and angles from refinements in Table 3. For clarity, error bars are not shown for the non-Ca olivines, but are generally quoted as near the size of the plotted points. The merwinite points at right are not plotted *vs.* ⟨M(1)–O⟩, but are shown for comparison with the olivine values. The error bars shown for merwinite and $\gamma$-$Ca_2SiO_4$ are one estimated standard deviation from positional parameters.

## *Assignment of high frequency modes*

*Symmetry coordinates.* In order to assign the observed bands to specific vibrational modes, it is useful to consider the internal stretching modes of the $SiO_4$ tetrahedra in terms of symmetry coordinates. When there is no coupling between these internal modes, the symmetry coordinates become identical with the normal coordinates. Figure 6 shows the symmetry coordinates of the modes derived from $\nu_1$ and $\nu_3$ vibrations of $SiO_4$, similar to those of Oehler and Günthard (1969). For forsterite, the frequency assignment given in this figure will be discussed in the following two sections, and clearly shows the effect of both Davydov and site-group spitting. The $\nu_1$-derived modes at 838 ($B_{3u}$) and 837.5 ($B_{2u}$), and the $\nu_3$-derived modes at 877 ($B_{3u}$) and 983 $cm^{-1}$ ($B_{2u}$) have net zero dipole moments from this schema, consistent with their observed low oscillator strengths. This also shows that the departure from pure symmetry coordinates is not too great, at least for infrared-active vibrations. This is not the case for the Raman-active modes observed in $A_g$ and $B_{1g}$ symmetries, as discussed below.

The $\nu_3$-derived motions give rise to three families of modes which may be distinguished with respect to the crystallographic axes. The first involves a motion parallel to *a* of silicon against the apical oxygen O(1) (second line in Figure 6). These give rise to the highest frequency modes within each symmetry, consistent with the observation that Si–O(1) is always the shortest distance in the olivine structure. The second type of vibration is predom-

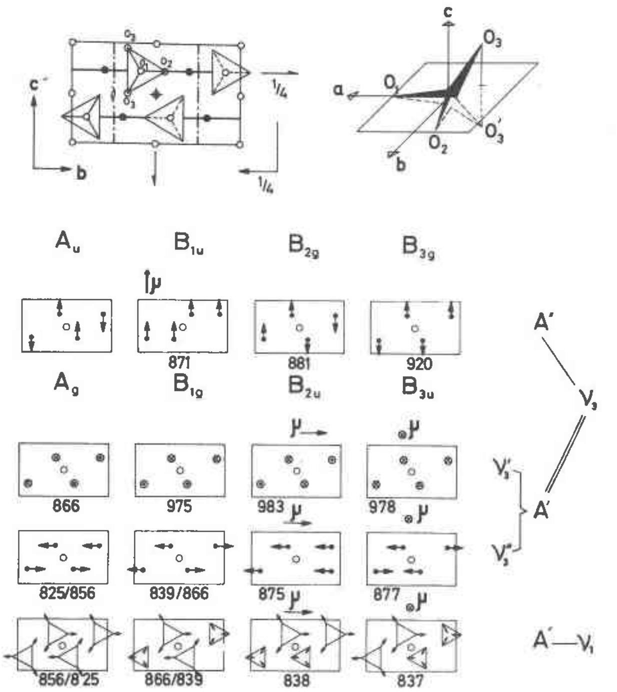

Fig. 6. Symmetry coordinates of high-frequency modes in forsterite. $\vec{\mu}$ is the induced dipole moment. A′ and A″ denote the types of motion relative to the $C_s$ symmetry of $SiO_4$ groups. Shown above are symmetry elements of the Pbnm space group relative to the unit cell, and the individual $SiO_4$ units.

inantly a movement of silicon against oxygen O(2) in the *b*-direction (third line in Figure 6). The Si–O(2) distance is the longest tetrahedral bond length in the olivines, and these bands are the lowest frequency $\nu_3$-derived modes. Finally, the motion of silicon in the *c*-direction is mainly against oxygens O(3), with an intermediate Si–O bond length, giving rise to a group of frequencies intermediate between the two families above.

*Infra-red results*. The bands in the 800–1000 $cm^{-1}$ region of orthosilicate crystal spectra may be attributed to modes derived from $\nu_1$ and $\nu_3$ internal vibrations of the $SiO_4$ tetrahedra. These bands have been assigned in a number of experimental and theoretical studies, but certain inconsistencies and points of disagreement persist among the results of different studies. These are discussed to allow a consistent band assignment. Infra-red reflection experiments have been carried out by Servoin and Piriou (1973) and Iishi (1978) for forsterite, by Stidham *et al.* (1976) for tephroite, and by Hohler and Funck (1969, 1973) for forsterite, tephroite and monticellite. Only Servoin and Piriou, and Iishi, carried out complete analyses of the reflection data by classical dispersion theory. Stidham *et al.* (1976) did not recalculate their reflection spectra to obtain mode frequencies, but used powder transmission data to estimate transverse optic (TO) mode frequencies, and the variation of reflection with angle of incidence (see below) to obtain approximate longitudinal (LO) frequencies. Hohler and Funck (1973) apparently took their mode frequencies at the maxima in their reflection spectra, hence their tabulated frequencies in Tables III–VI are overestimated and incorrect, although their reflection data are of good quality. Iishi (1978) used his results for a normal mode analysis of forsterite, while Devarajan and Funck (1975) carried out a similar calculation using the infrared data of Servoin and Piriou (1973), and the Raman spectra of Hohler and Funck (1973). There is some disagreement among the above experimental studies related to the presence of extra modes in some spectra and relative band intensities, which may be simply reconciled.

When a weak mode is present near a stronger band of slightly higher frequency, the oscillator strength of the weak mode may be overestimated to the detriment of the stronger band, without noticeable effect on the fit of experimental and calculated spectra. If the data of Servoin and Piriou (1973) and Iishi (1978) for the pair of $B_{2u}$ modes at 875 and 838 $cm^{-1}$ are compared, the oscillator strength of the weaker mode seems better reproduced by Iishi ($\Delta\varepsilon$ = 0.08). A similar transfer of intensity has occurred for the $B_{3u}$ modes observed at 978 and 952 $cm^{-1}$. However, the 952 $cm^{-1}$ frequency may be an artifact in the $B_{3u}$ spectrum, as discussed below.

Comparison of all the experimental reflection spectra above reveals a number of modes not predicted by theory in some spectra, which are not always observed, and which vary in relative intensity between authors. For anisotropic crystals, the infrared reflection spectrum becomes a non-linear combination of modes of different symmetries when the incident beam does not coincide with a principal crystallographic axis (*e.g.*, Alain and Piriou, 1971). For a given experimental configuration, one can show that the response function Im $(1/\varepsilon)$ (resonance function for LO modes in a spectrum of pure symmetry) gives rise to maxima at the frequencies of LO modes involved in the quasi-spectra above, independent of their symmetry. It follows that the reflection spectra of these quasi-modes show minima near the frequencies of each LO mode in the combination spectrum, which become more marked with increasing LO mode intensity (with a greater peak surface in Im $(1/\varepsilon)$). This was used by Stidham *et al.* (1976) in an attempt to determine their LO mode frequencies for tephroite. For measurements in normal incidence, the beam aperture and small orientation errors may lead to the appearance of artifacts, due to strong LO modes of one symmetry leaking into spectra of another nominal symmetry. This may be observed in the reflection spectra for the olivines, and accounts for the extra modes at 957 $cm^{-1}$ ($B_{3u}$: LO of $B_{2u}$ at 962.5), 962 $cm^{-1}$ ($B_{1u}$: LO of $B_{2u}$ at 962.5) and 1030 $cm^{-1}$ ($B_{2u}$: LO of $B_{3u}$ at 1081), which may be eliminated.

The 957 $cm^{-1}$ frequency was taken into account by Iishi (1978) as a TO mode in his normal mode calculation. This may explain the incompatibility of the experimental oscillator strength at $\Delta\varepsilon$ = 0.12 and the small calculated TO–LO splitting (less than 1 $cm^{-1}$, independent of the model used), and the general poor fit of observed and calculated $\nu_3$-derived frequencies. On the other hand, the weak $B_{3u}$ mode only observed by Servoin and Piriou (1973) at 877 cm$^{-1}$ (TO–LO splitting of 1 cm$^{-1}$) was not considered by Iishi although it is probably the second $\nu_3$ component in $B_{3u}$ symmetry. This is consistent with the calculation of Devarajan and Funck (1975), who ignored the 957 cm$^{-1}$ frequency and used the $B_{3u}$ mode at 877 cm$^{-1}$, to obtain a better fit of the Davydov splitting. The above discussion also applies to the $B_{3u}$ spectrum of Stidham *et al.* (1976) for tephroite, where the true, weak $B_{3u}$ mode was not observed, and the apparent $B_{3u}$ frequency at 914 cm$^{-1}$ corresponds to leakage of a strong LO component from the $B_{2u}$ spectrum.

*Raman results*. For forsterite, Griffith (1969) assigned the 826 cm$^{-1}$ Raman band to $\nu_1$, and that near 860 cm$^{-1}$ to $\nu_3$, based on their relative intensities. However, in his Table 2, both modes appear as "strong" bands. The relative intensities of these bands vary with sample orientation, as seen from the single crystal studies of Servoin and Piriou (1973) and Iishi (1978). The $Mn_2SiO_4$ sample of Stidham *et al.* (1976) showed a similar relative intensity variation for the two most intense $A_g$ modes. The relative intensities of these bands cannot then be simply used to distinguish their $\nu_1$- or $\nu_3$-derived character.

Several authors (*e.g.*, Tarte, 1963; Toropov *et al.*, 1963) have tabulated the variation of $\nu_1$ and $\nu_3$ frequencies of orthosilicates from infrared measurements against mean cation radius. It was shown by White (1975) that such plots did not show any simple systematics. (However, see later in this discussion.) For this study it was thought that following the Raman spectra through the olivine series $Mg_2SiO_4$–$CaMgSiO_4$–$\gamma$-$Ca_2SiO_4$ might show systematic differences between the two bands in question, giving support to some attribution. As seen from Figures 1 and 7 and Table 2, the two bands of interest appear to vary in a similar way along the series, allowing no distinction between them.

The results of vibrational calculations for olivines do not allow the $\nu_1$- and $\nu_3$-derived $A_g$ modes to be distinguished either. In their vibrational analysis for forsterite, Devarajan and Funck (1975) assigned the $A_g$ 822 cm$^{-1}$ band to $\nu_1$, as for the $B_{1g}$ ($B_{2g}$ in the Devarajan–Funck coordinate system) at 835 cm$^{-1}$. The original fit was poor, even for internal modes of $SiO_4$, and a new fit was made using the correct ($C_s$) symmetry for the $SiO_4$ units, with "corresponding" force constants. The $\nu_3$ band at 960 cm$^{-1}$ shared the same set of force constants as their $\nu_1$ band at 835 cm$^{-1}$ while a different set appeared for their $\nu_3$ band at 854 cm$^{-1}$. This apparent reversal of roles was observed for other $\nu_1$ and $\nu_3$ force constant sets. On closer examination of the main force constant sets, each one appeared based only on $\nu_3$-type motions, involving stretching of three out of four Si–O bonds, along with an angular O–Si–O interaction constant. No set corresponding to $\nu_1$-type vibrations was found, which might have been expected, even with a nontetrahedral $SiO_4$ unit. These authors noted some difficulty with their force constant refinement. The calculation of Iishi (1978) also chose $\nu_1$ as his 826 cm$^{-1}$ band, and the associated $B_{1g}$ at 839 cm$^{-1}$. This calculation did not give good agreement with experiment for high frequency Raman-active modes, and none of the displacement vectors reflect pure $\nu_3$-type motions.

Finally, Pâques-Ledent and Tarte (1973) carried out $^{28}Si$–$^{30}Si$ isotopic substitution experiments on $Mg_2SiO_4$, and obtained Raman spectra in an attempt to definitely assign the 826 and 855 cm$^{-1}$ bands. They cited Griffith (1969) as having chosen 855 cm$^{-1}$ as $\nu_1$ (he in fact chose 826 cm$^{-1}$) for its intensity. The $\nu_1$-derived band should involve much less movement of Si than $\nu_3$-derived vibrations, even for distorted tetrahedra, and hence such an isotopic experiment should discern the $\nu_1$- and $\nu_3$-derived modes. Pâques-Ledent and Tarte concluded that, since all bands showed an isotope effect, the two bands in question must have mixed $\nu_1$–$\nu_3$ character. We generally agree with this conclusion, but note also that the 855 cm$^{-1}$ band shifted less than the others, suggesting more $\nu_1$-character for this mode. This is also consistent with the earlier comparison of $CaMgSiO_4$ glass and crystal spectra, which suggested $\nu_1$-character for the 852 cm$^{-1}$ mode of monticellite due to its coincidence with the glass band assigned to $\nu_1$. It is of interest that Pâques-Ledent and Tarte found the expected isotopic shifts for their infrared experiment, suggesting that $\nu_1$–$\nu_3$ coupling is less important for IR-active bands than for Raman-active vibrations in the olivines. This was also suggested by the comparison of symmetry and normal coordinates for infrared vibrations considered above.

## Vibrational mode coupling

From the isotopic exchange studies, it is obvious that there exists considerable coupling between Raman-active $\nu_1$–$\nu_3$-derived vibrations of similar frequency. This coupling may be better understood by consideration of a simple system of two coupled harmonic oscillators, characterized by their coordinates $x_1$ and $x_2$ and a coupling constant $\beta^2$. The equations of motion are:

$$\ddot{x}_1 + \omega_1^2 x_1 - \beta^2 x_2 = 0$$

$$\ddot{x}_2 + \omega_2^2 x_2 - \beta^2 x_1 = 0$$

where $\omega_1$ and $\omega_2$ are the resonant frequencies in the absence of coupling (referred to below as the "pure" frequencies). Solution of this system of simultaneous equations leads to the two eigenfrequencies $\Omega_+$ and $\Omega_-$, where

$$\Omega_\pm^2 = \frac{\omega_1^2 + \omega_2^2}{2} \pm \left[\left(\frac{\omega_1^2 + \omega_2^2}{2}\right)^2 + \beta^4\right]^{1/2} \qquad (1)$$

The normal coordinates $Q_\pm$ corresponding to the coupled frequencies $\Omega_\pm$ are given by:

$$Q_+ = a_1x_1 - a_2x_2 \tag{2a}$$

$$Q_- = a_2x_1 + a_1x_2 \tag{2b}$$

where

$$a_1 = \frac{\beta^2}{\beta^2 + \Omega_+^2 - \omega_1^2} \tag{3a}$$

and

$$a_2 = \frac{\beta^2}{\beta^2 - \Omega_-^2 + \omega_1^2} \tag{3b}$$

if one normalizes $a_1 + a_2 = 1$. From these expressions, the two oscillators vibrate in opposition for the higher frequency mode $\Omega_+$, and in phase for $\Omega_-$ at lower frequency. In the following discussion, we neglect damping terms for simplicity, which should not greatly affect the eigenfrequencies, nor the relation between $a_1$ and $a_2$.

If for a given coupling, the pure frequencies $\omega_1$ and $\omega_2$ vary with some physical parameter X, it remains possible to calculate the coupled frequencies $\Omega_+$ and $\Omega_-$. For instance, this is the case for structures with coupled modes of which one shows soft mode behavior (*e.g.*, Alain and Piriou, 1977). In the case of the olivines, a number of studies have considered the variation of IR and Raman bands with composition (Tarte, 1963; Toropov *et al.*, 1963; Duke and Stephens, 1964; Burns and Huggins, 1972; White, 1975; this work, Figure 7). It is evident that both $\nu_1$- and $\nu_3$-derived modes show a general decrease in frequency from forsterite to $\gamma$-$Ca_2SiO_4$, while the site-group splitting of the $\nu_3$-derived vibrations also appears to decrease. The structural factors responsible for these changes may be embodied in some parameter X, with which the pure, uncoupled frequencies $\omega_i$ are assumed to vary linearly. The pure (uncoupled) frequencies for the three $A_g$ modes derived from $\nu_1$ and $\nu_3$ motions are assumed to be: $\omega_1 = 858$, $\omega_2 = 848$ and $\omega_3 = 993$ cm$^{-1}$. These frequencies are assumed to vary as $\omega_1(\text{cm}^{-1}) = 858 - 24X$; $\omega_2(\text{cm}^{-1}) = 848 - 11.5X$; $\omega_3(\text{cm}^{-1}) = 993 - 43.5X$, as shown in Figure 8. Modes $\omega_1$ and $\omega_2$ are strongly coupled, and Figure 8 shows the variation of the coupled frequencies $\Omega_+$ and $\Omega_-$ with X for a coupling constant $\beta = 160$ cm$^{-1}$. Also shown in Figure 8 are the observed high-frequency $A_g$ modes for forsterite, monticellite, tephroite and $\gamma$-$Ca_2SiO_4$ from Table 2, placed so that the highest frequency mode observed lies on the line calculated for $\omega_3$. The calculated coupled frequencies for $\Omega_+$ and $\Omega_-$ show reasonable agreement with the experimental frequencies for the remaining two $\nu_1$- and $\nu_3$-derived modes. We note, however, that this coupling diagram is only intended to be schematic. We have no way of relating the parameter X to structural effects within the olivines, and the variations of $\omega_1$, $\omega_2$ and $\omega_3$ are not necessarily linear functions of X. Finally, the "pure" frequencies $\omega_1$, $\omega_2$ and $\omega_3$ were only estimated for this discussion, while the coupling parameter $\beta$ need not necessarily be constant. The diagram does indicate that a simple coupling scheme may be used to describe the $\nu_1$- and $\nu_3$-derived Raman-active modes in the olivine series.

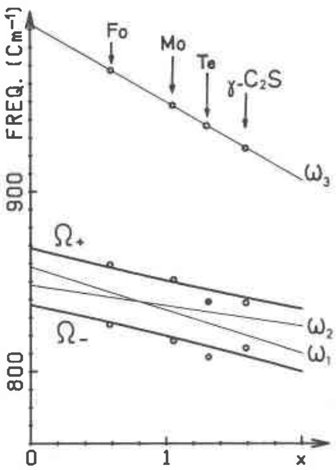

Fig. 8. Schematic coupling diagram for high-frequency modes of the olivine structure, applicable to $A_g$ and $B_{1g}$ species. This may be compared with the observed frequency variation in Figure 7. The parameters X, $\omega_1$, $\omega_2$, $\omega_3$, $\Omega_+$ and $\Omega_-$ are explained in the text.

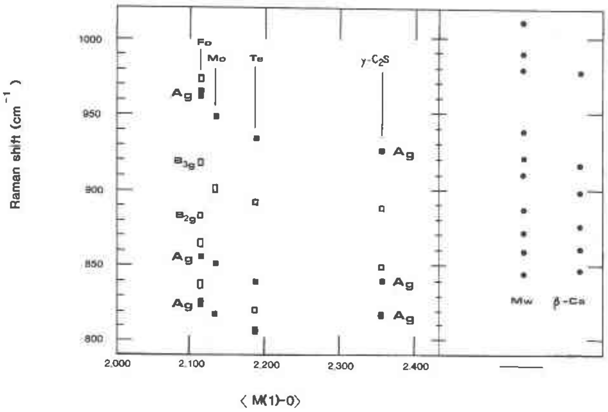

Fig. 7. Variation with ⟨M(1)–O⟩ of Raman frequencies from Table 2. The merwinite and larnite points are not plotted *vs.* ⟨M(1)–O⟩, but are shown for comparison with the olivine values. The size of the points for Raman frequencies represents the range of observed values from the studies quoted in Table 2. $A_g$ modes are shown by full rectangles: other symmetries by boxes.

Figure 7 shows the observed Raman frequencies for forsterite, monticellite, tephroite and $\gamma$-$Ca_2SiO_4$ plotted against the average M(1)–O bond length, as for the structural parameters discussed earlier. This may be compared with the schematic coupling scheme in Figure 8. It is beyond the scope of this article to discuss the coupling in detail, since both pure $\nu_1$- and $\nu_3$-derived band frequencies and the coupling parameter must vary in a complex way with composition, being dependent on a variety of structural and dynamic factors.

The proposed coupling scheme implies a cross-over of modes of $\nu_1$- and $\nu_3$-type which may be justified as follows. The calcic olivine $\gamma$-$Ca_2SiO_4$ was shown earlier to have the most regular $SiO_4$ tetrahedral units, hence the least $\nu_1$-$\nu_3$ coupling, while the degree of coupling should increase through tephroite and monticellite to forsterite. The $\nu_1$-derived mode of $\gamma$-$Ca_2SiO_4$ was found near 815 $cm^{-1}$ in the powder infrared studies of Tarte (1963) and Oehler and Günthard (1969). This suggests the attribution of the strong $A_g$ Raman mode near 815 $cm^{-1}$ (Boyer in publicity for Jobin-Yvon MOLE: see notes to Table 2; this study, Figure 1) to a $\nu_1$-type vibration in a system with little $\nu_1$–$\nu_3$ coupling. On the other hand, the isotopic studies on forsterite (Pâques-Ledent and Tarte, 1973) showed that the $A_g$ Raman band at 855 $cm^{-1}$ had more $\nu_1$ character than the strong $A_g$ mode at lower frequency, although both are strongly coupled. These observations agree with a coupling scheme with cross-over of bands of pure $\nu_1$ and $\nu_3$ character, as drawn in Figure 8.

When X is small, the normal coordinates $Q_+$ and $Q_-$ (Equation 2) are dominated by $x_1$ and $x_2$ respectively. This is reversed for large X, with a continuous transfer of character, as described by the linear equations. The Raman intensity of the $\nu_1$- and $\nu_3$-derived $A_g$ modes is related to their proportion of $\nu_1$ character. This may be seen from Figure 1, where the highest-frequency $A_g$ mode has little $\nu_1$-character, and is much less intense than the other two $A_g$ modes. These two intense $A_g$ modes undergo a transfer of Raman intensity in the series forsterite–monticellite–$\gamma$-$Ca_2SiO_4$ (Fig. 1), which is in agreement with the coupling scheme of Figure 8, where $\chi_1$ and $\chi_2$ correspond to the symmetry coordinates relative to $\nu_1$ and $\nu_3$ shown in Figure 6. We consider that $\gamma$-$Ca_2SiO_4$ is least affected by $\nu_1$–$\nu_3$ coupling, with its strong $A_g$ band of lower frequency being predominantly $\nu_1$ in character. As the coupling increases towards forsterite, the higher frequency strong $A_g$ band takes on more $\nu_1$ character, transferring $\nu_3$ character to the lowest frequency $A_g$. The olivines monticellite and tephroite lie in a region of strong $\nu_1$–$\nu_3$ coupling, where neither band has well-defined character. The two strong $A_g$ bands for monticellite are nearly equal in intensity (Fig. 1), suggesting that monticellite lies near the crossover point of $a_1$ and $a_2$ (Fig. 9) where both modes have equal $\nu_1$- and $\nu_3$-character. This implies that the coincidence of the 854 $cm^{-1}$ mode in monticellite glass and crystal discussed earlier is fortuitous. The above model will also hold for the $B_{1g}$ modes associated with the $A_g$ vibrations by the Davydov splitting.

The coupling scheme does not appear so simple for the infra-red active vibrations. The $\nu_1$-derived IR band for $\gamma$-$Ca_2SiO_4$ appears weak in the powder spectra of Tarte (1963) and Oehler and Günthard (1969), consistent with little $\nu_1$–$\nu_3$ coupling as above, and increases in intensity for monticellite, tephroite and fayalite (Tarte, 1963; Burns and Huggins, 1972) as expected. However, this band then decreases in intensity between fayalite and forsterite, suggesting a decrease in $\nu_1$–$\nu_3$ coupling. The IR-active bands do not show a frequency cross-over and change of character as do the Raman spectra, suggesting a more complex coupling scheme for the olivine infrared spectra. However, it was noted earlier that vibrational mode coupling cannot be important in these spectra, from a consideration of band intensities.

## *Relationship between orthosilicate high-frequency bands and structure*

This final section considers a number of general correlations between the structure and high-frequency vibrational spectra of olivines and related orthosilicates. It was noted earlier that the frequencies of $\nu_1$- and $\nu_3$-derived modes in olivine decreased with increasing M(1) cation size, which may be correlated with the general increase in average Si–O bond length from forsterite to $\gamma$-$Ca_2SiO_4$ (Figure 5a). This may be contrasted with comparable glass spectra, where the $\nu_1$ frequency was found to vary little with composition. The $\nu_1$-derived modes for the olivine structure $\gamma$-$Ca_2SiO_4$ are found near 815 $cm^{-1}$ compared with 860 $cm^{-1}$ for $\nu_1$ of $SiO_4$ in calcium silicate glasses. However, a strong band is found in the Raman spectrum of larnite near 860 $cm^{-1}$ ($\beta$-$Ca_2SiO_4$; Fig. 2) which may be assigned to a $\nu_1$-derived $A_g$ mode in this non-olivine structure. We suggest that formation of $\gamma$-$Ca_2SiO_4$ with its high degree of polyhedral edge-sharing results in an expansion of the $SiO_4$ tetrahedra to accomodate the large $Ca^{2+}$ on both M(1) and M(2) sites, and is responsible for the lowered Si–O stretching frequencies. The larnite structure has much less tetrahedral–octahedral edge-sharing, and allows the $SiO_4$ tetrahedra to relax to approximately their free-ion geometry, with a central stretch frequency similar to that in the glass. The available structure refinement for $\beta$-$Ca_2SiO_4$ is not precise enough to confirm this for the tetrahedral Si–O distances.

Merwinite ($Ca_3MgSi_2O_8$) has no shared polyhedral edges, and its average Si–O distances are less than those for the olivines (Fig. 5a). This is manifested in its Raman

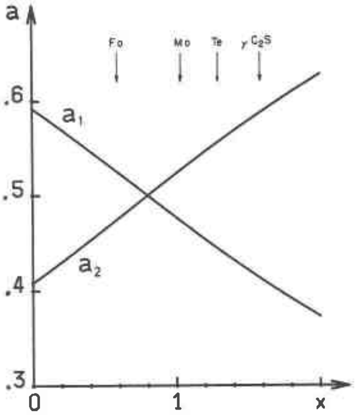

Fig. 9. Variation of the coefficients $a_1$ and $a_2$, which determine the relative character of $\omega_1$ and $\omega_2$, with X for the same conditions as Figure 8.

spectrum (Fig. 2b; Table 2), where the silicate stretch vibrations appear at higher frequencies than for the olivines. Similarily, tricalcium silicate ($Ca_3SiO_5$) contains $SiO_4$ units linked only by their corners to calcium–oxygen polyhedra, with mean Si–O distances smaller than in the olivines (Golovastikov *et al.,* 1976). Its principal, and presumably $\nu_1$-derived, Raman bands occur at 845 and 855 $cm^{-1}$ (Conjeaud and Boyer, 1980), near that of $\nu_1$ in the glass.

Not only do the absolute frequencies of Si–O stretch vibrations decrease along the olivine series from forsterite to $\gamma$-$Ca_2SiO_4$, but also the site-group splitting of the $\nu_3$-derived modes (Fig. 7). As the $SiO_4$ unit is distorted from tetrahedral symmetry, this splitting is expected to increase, although the $\nu_1$–$\nu_3$ coupling discussed above may complicate this behavior. The observed decrease in $\nu_3$ splitting may be related to the converging trends of tetrahedral distances and angles as M(1) becomes larger (Fig. 5), giving a more symmetric $SiO_4$ unit as $\gamma$-$Ca_2SiO_4$ is approached. Jeanloz (1980) has compared the infrared spectra of a number of silicate olivines and spinels. In the cubic spinel structure, the $SiO_4$ unit has tetrahedral symmetry (Brown, 1980), and no splitting of $\nu_3$-type vibrations would be expected. The spinel spectra showed a single major high-frequency band which Jeanloz (1980) assigned to $\nu_3$ motions of $SiO_4$, with weaker bands attributed to tetrahedral-octahedral site vibrational interactions. The reduction in $\nu_3$ splitting with increase in $SiO_4$ symmetry is consistent with the above discussion for the olivine series.

## Conclusion

This study began as a simple comparison of $CaMgSiO_4$ glass and its corresponding crystal, but since grew into a survey of the vibrational spectroscopic and structural literature on the olivines. We have attempted to identify a consistent set of high-frequency Raman and infrared modes for olivine, with suggested assignments to vibrational types. We suggest that vibrational mode coupling between $\nu_1$- and $\nu_3$-derived vibrations is important for the Raman-active $A_g$ and related $B_{1g}$ modes, but less so for infrared-active modes. This should be taken into account in future lattice dynamical calculations, along with the correct band assignments. Frequency shifts of $\nu_1$- and $\nu_3$-derived modes, and the degree of $\nu_3$ splitting, may be correlated with systematic changes in the geometry of the $SiO_4$ unit, although these may be complicated by $\nu_1$–$\nu_3$ coupling. Finally, it seems that the original point of this study—the coincidence of the Raman band near 850 $cm^{-1}$ in $CaMgSiO_4$ crystal and glass—is entirely fortuitous. We suggest that the two intense $A_g$ modes in the monticellite spectrum have almost equal $\nu_1$ and $\nu_3$ character, while that for $CaMgSiO_4$ glass is pure $\nu_1$.

## Acknowledgments

The authors gratefully acknowledge support from the French CNRS and the PIRPSEV program, and from the National Science Foundation (grants EAR-78-09954-02 and INT-79-26523). We thank G. M. Biggar for providing the $CaMgSiO_4$ gel, J. P. Coutures for help with the solar furnace preparations, and J. Etchepare for the use of his Raman laboratory for the merwinite spectrum. We are grateful to J. Clark, J. Bradley and A. Yates for their assistance with sample analyses, carried out in the Chemistry Department at A.S.U.. A. Navrotsky and J. Holloway read and commented on original versions of this manuscript, which was typed by V. Rehder, N. Dagon and M. Palitz. Finally, we thank R. Jeanloz, G. Rossman and an anonymous reviewer for their helpful and constructive criticisms.

## References

Aden, G. D. and Buseck, P. R. (1979). Rapid quantitative analysis of individual particles by energy-dispersive spectrometry. In D. E. Newbury, Ed., Microbeam Analysis, p. 254–258. San Francisco Press Inc.

Alain, P. and Piriou, B. (1971). Etude infrarouge et Raman des vibrations de réseau de L'Aluminate de Néodyme. Physica Status Solidi, 43, 669–680.

Alain, P. and Piriou, B. (1977). Transition de phase à haute temperature dans les aluminates de terre rare. Journal de Physique, 12, C7, 389–394.

Basso, R., Dal Negro, A., Della Giustia, A. and Rossi, G. (1979). Fe/Mg distribution in the olivine of ultramafic nodules from Assab (Ethiopia). Neues Jahrbuch für Mineralogie, Monatshefte, 5, 197–202.

Biggar, G. M. and O'Hara, M. J. (1969). Monticellite and forsterite crystalline solutions. Journal of the American Ceramic Society, 52, 249–252.

Birle, J. D., Gibbs, G. V., Moore, P. B. and Smith, J. V. (1968). Crystal structures of natural olivines. American Mineralogist, 53, 807–824.

Bretheau-Raynal, F., Dalbiez, J. P., Drifford, M. and Blanzat, B. (1979). Raman spectroscopic study of thortveitite structure silicates. Journal of Raman Spectroscopy, 8, 39–42.

Brown, G. E. (1970). The crystal chemistry of the olivines. Ph.D. Thesis, Virginia Polytechnic Institute and State University, Blacksburg, Virginia (not seen: referenced data appears in Brown (1980)).

Brown, G. E. (1980). Olivines and silicate spinels. In P. H. Ribbe, Ed., Orthosilicates, p. 275–381. Reviews in Mineralogy, Volume 5, Mineralogical Society of America.

Brown, G. E. and Prewitt, C. T. (1973). High temperature crystal chemistry of hortonolite. American Mineralogist, 58, 577–587.

Burns, R. G. and Huggins, F. E. (1972). Cation determinative curves for Mg–Fe–Mn olivines from vibrational spectra. American Mineralogist, 57, 967–985.

Conjeaud, M. and Boyer, H. (1980). Some possibilities of Raman microprobe in cement chemistry. Cement and Concrete Research, 10, 61–70.

Coons, W. E. (1978). Cobalt as an analogue for iron in high temperature experiments on basaltic compositions. Ph.D. Thesis, Arizona State University, Tempe, Arizona.

Coutures, J. P., Berjoan, R., Benezech, G. and Granier, B. (1978). Utilisation des fours solaires de laboratoire pour l'étude à haute temperature des propriétés physicochimiques des oxydes refractaires. Revue Internationale des Hautes Temperatures et Refractaires, 15, 103–114.

Cruikshank, D. W. J. (1964). Refinements of structures containing bonds between Si, P, S or Cl and O or N. X. $\beta$-$Ca_2SiO_4$.

Acta Crystallogaphica, 17, 685–686.

Czaya, R. (1971). Refinement of the structure of $\gamma$-$Ca_2SiO_4$. Acta Crystallogaphica, B27, 848–849.

Devarajan, V. and Funck, E. (1975). Normal coordinate analysis of the optically active vibrations (k=0) of crystalline magnesium orthosilicate $Mg_2SiO_4$ (forsterite). Journal of Chemical Physics, 62, 3406–3411.

Duke, D.A. and Stephens, G. D. (1964). Infrared investigation of the olivine group minerals. American Mineralogist, 49, 1388–1406.

Eysel, W. and Hahn, T. (1970). Polymorphism and solid solution of $Ca_2GeO_4$ and $Ca_2SiO_4$. Zeitschrift für Kristallographie, 131, 322–341.

Fateley, W. G., Dollish, F. R., McDevitt, N. T. and Bentley, F. F. (1972). Infrared and Raman selection rules for molecular and lattice vibrations: the correlation method. Wiley-Interscience, New York.

Finger, L. W. (1970). Fe/Mg ordering in olivines. Carnegie Institute of Washington Year Book, 69, 302–305.

Fortnum, D. and Edwards, J. O. (1956). The Raman spectrum and the structure of the aqueous silicate ion. Journal of Inorganic and Nuclear Chemistry, 2, 264–265.

Francis, C. A. and Ribbe, P. H. (1980). The forsterite–tephroite series: I. Crystal structure refinements. American Mineralogist, 65, 1263–1269.

Ghose, S. and Wan, C. (1974). Strong site preference of $Co^{2+}$ in olivine, $Co_{1.10}Mg_{0.90}SiO_4$. Contributions to Mineralogy and Petrology, 47, 131–140.

Golovastikov, N. I., Matveeva, R. G. and Belov, N. V. (1976). Crystal structure of the tricalcium silicate $3CaO \cdot SiO_2 = C_3S$. Soviet Physics Crystallography, 20, 441–445.

Griffith, W. P. (1969). Raman spectroscopy of minerals. Nature, 224, 264–266.

Handke, M. and Ptaak, W. (1978). I.R. and Raman studies of the stabilization of $\beta$-$Ca_2SiO_4$. Ceramurgia International, 4, 75–78.

Hanke, K. (1965). Beiträge zu Kristallstrukturen vom Olivin-Typ. Beiträge zur Mineralogie und Petrographie, 11, 535–558.

Hazen, R. M. (1976). Effects of temperature and pressure on the crystal structure of forsterite. American Mineralogist, 61, 1280–1293.

Hazen, R. M. (1977). Effects of temperature and pressure on the crystal structure of ferromagnesian olivine. American Mineralogist, 62, 286–295.

Heinrich, K. F. J. (1972). A simple correction procedure for quantitative electron probe microanalysis. National Bureau of Standards Technical Note 719, U. S. Government Printing Offices.

Herzberg, G. (1945). Molecular Spectra and Molecular Structure. II. Infrared and Raman spectra of polyatomic molecules. Van Nostrand, New York.

Hohler, V. and Funck, E. (1969). Infrarot-Spektrum von Sinhalit und Olivin. Naturwissenschaften, 56, 459.

Hohler, V. and Funck, E. (1973). Vibrational spectra of crystals with olivine structure. I. Silicates. Zeitschrift für Naturforschung B, 28, 125–139.

Iishi, K. (1978). Lattice dynamics of forsterite. American Mineralogist, 63, 1198–1208.

Jeanloz, R. (1980). Infrared spectra of olivine polymorphs: $\alpha$, $\beta$ phase and spinel. Physics and Chemistry of Minerals, 5, 327–341.

Kashio, S. Iguchi, Y., Goto, T., Nishina, Y. and Fuwa, T. (1980). Raman spectroscopic study on the structure of silicate slag. Transactions of the Iron and Steel Institute of Japan, 20, 251–253.

Kusabiraki, K. and Shiraishi, Y. (1981). The infrared spectrum of vitreous fayalite. Journal of Non-Crystalline Solids, 44, 365–368.

Lager, G. A. and Meagher, E. P. (1978). High-temperature structural study of six olivines. American Mineralogist, 63, 365–377.

Lazarev, A. N. (1972). Vibrational spectra and structure of silicates. Consultants Bureau, New York.

Louisnathan, S. J. and Gibbs, G. V. (1972). Variation of Si–O distances in olivines, soda melilite and sodium metasilicate as predicted by semiempirical molecular orbital calculations. American Mineralogist, 57, 1643–1663.

McMillan, P. (1981). A structural study of aluminosilicate glasses by Raman spectroscopy. Ph.D. Dissertation, Arizona State University, Tempe, Arizona.

McMillan, P., Coutures, J. P. and Piriou, B. (1981). Diffusion Raman d'un verre de monticellite. Comptes Rendus de l'Academie de Sciences à Paris, Série II, 292, 195–198.

Midgley, C. M. (1952). The crystal structure of $\beta$ dicalcium silicate. Acta Crystallographica, 5, 307–312.

Moore, P. B. and Araki, T. (1972). Atomic arrangement of merwinite, $Ca_3Mg(SiO_4)_2$, an unusual dense-packed structure of geophysical interest. American Mineralogist, 57, 1355–1374.

Morimoto, N., Tokonami, M., Watanabe, M. and Koto, K. (1974). Crystal structures of three polymorphs of $Co_2SiO_4$. American Mineralogist, 59, 475–485.

Mysen, B. O., Virgo, D. and Scarfe, C. M. (1980). Relations between the anionic structure and viscosity of silicate melts—a Raman spectroscopic study. American Mineralogist, 65, 690–710.

Nelson, B. N. and Exarhos, G. J. (1979). Vibrational spectroscopy of cation-site interactions in phosphate glasses. Journal of Chemical Physics, 71, 2739–2747.

Oehler, O. and Gunthard, Hs.H. (1969). Low-temperature infrared spectra between 1200 and 20 $cm^{-1}$ and normal-coordinate analysis of silicates with olivine structure. Journal of Chemical Physics, 51, 4719–4727.

Onken, H. (1965). Verfeinerung der Kristallstruktur von Monticellite. Tschermaks Mineralogische und Petrographische Mitteilungen, 10, 34–44.

Pâques-Ledent, M.Th. and Tarte, P. (1973). Vibrational studies of olivine-type compounds—I. The i.r. and Raman spectra of the isotopic species of $Mg_2SiO_4$. Spectrochimica Acta, 29A, 1007–1016.

Rajamani, V., Brown, G. E. and Prewitt, C. T. (1975). Cation ordering in Ni–Mg olivine. American Mineralogist, 60, 292–299.

Servoin, J. L. and Piriou B. (1973). Infrared reflectivity and Raman scattering of $Mg_2SiO_4$ single crystal. Physica Status Solidi (b), 55, 677–686.

Smyth, J. R. (1975). High temperature crystal chemistry of fayalite. American Mineralogist, 60, 1092–1097.

Smyth, J. R. and Hazen, R. M. (1973). The crystal structures of forsterite and hortonolite at several temperatures up to 900°C. American Mineralogist, 58, 588–593.

Stidham, H. D., Bates, J. B. and Finch, C. B. (1976). Vibrational spectra of synthetic single crystal tephroite, $Mn_2SiO_4$. Journal of Physical Chemistry, 80, 1226–1234.

Tarte, P. (1963). Etude infra-rouge des orthosilicates et des orthogermanates—II. Structures du type olivine et monticellite. Spectrochimica Acta, 19, 25–47.

Thomas, I. L. and Haukka, M. T. (1978). XRF determination of trace and major elements using a single-fused disc. Chemical Geology, 21, 39–50.

Toropov, N. A., Fedorov, N. F. and Shevyakov, A. M. (1963). Infrared absorption spectra of orthosilicates of some bivalent elements. Russian Journal of Inorganic Chemistry, 8(6), 697–699.

Virgo, A., Mysen, B. O. and Kushiro, I. (1980). Anionic constitution of silicate melts quenched at 1 atm from Raman spectroscopy: Implications for the structure of igneous melts. Science, 208, 1371–1373.

Warner, R. D. and Luth, W. C. (1973). Two-phase data for the join monticellite ($CaMgSiO_4$)–forsterite ($Mg_2SiO_4$): Experimental results and numerical analysis. American Mineralogist, 58, 1009–1015.

Wenk, H.-R. and Raymond, K. N. (1973). Four new structure refinements of olivine. Zeitschrift für Kristallographie, 137, 86–105.

White, W. B. (1975). Structural interpretations of lunar and terrestrial minerals of Raman spectroscopy. In C. Karr, Ed., Infrared and Raman spectroscopy of lunar and terrestrial materials, p. 325–358, Academic Press, New York.

Yamaguchi, G. and Suzuki, K. (1967). Structural analysis of merwinite. Journal of the Ceramic Association of Japan, 75, 220–229.

*Manuscript received, April 2, 1982;*
*accepted for publication, September 20, 1982.*